7. SITE 1013[1]

Shipboard Scientific Party[2]

HOLE 1013A

Date occupied: 5 May 1996

Date departed: 6 May 1996

Time on hole: 16 hr, 00 min

Position: 32°48.040′N, 118°53.922′W

Drill pipe measurement from rig floor to seafloor (m): 1575.4

Distance between rig floor and sea level (m): 11.0

Water depth (drill pipe measurement from sea level, m): 1564.4

Total depth (from rig floor, m): 1721.5

Penetration (m): 146.1

Number of cores (including cores having no recovery): 16

Total length of cored section (m): 146.1

Total core recovered (m): 137.1

Core recovery (%): 93.0

Oldest sediment cored:
Depth (mbsf): 146.10
Nature: Nannofossil ooze, clayey nannofossil ooze
Age: late Pliocene

Measured velocity (km/s): 1.567 at Section 4H-3, 111–114 cm

HOLE 1013B

Date occupied: 6 May 1996

Date departed: 6 May 1996

Time on hole: 07 hr, 30 min

Position: 32°48.059′N, 118°53.927′W

Drill pipe measurement from rig floor to seafloor (m): 1574.4

Distance between rig floor and sea level (m): 11.0

Water depth (drill pipe measurement from sea level, m): 1563.4

Total depth (from rig floor, m): 1678.2

Penetration (m): 103.8

Number of cores (including cores having no recovery): 11

Total length of cored section (m): 103.8

Total core recovered (m): 108.0

Core recovery (%): 104.0

Oldest sediment cored:
Depth (mbsf): 103.80
Nature: Clayey nannofossil mixed sediment, clayey nannofossil ooze
Age: late Pliocene

HOLE 1013C

Date occupied: 6 May 1996

Date departed: 6 May 1996

Time on hole: 07 hr, 15 min

Position: 32°48.061′N, 118°53.917′W

Drill pipe measurement from rig floor to seafloor (m): 1575.8

Distance between rig floor and sea level (m): 11.0

Water depth (drill pipe measurement from sea level, m): 1564.8

Total depth (from rig floor, m): 1648.0

Penetration (m): 72.2

Number of cores (including cores having no recovery): 8

Total length of cored section (m): 72.2

Total core recovered (m): 74.0

Core recovery (%): 102.0

Oldest sediment cored:
Depth (mbsf): 72.20
Nature: Clay with nannofossils and nannofossil ooze with silt and foraminifers
Age: Pleistocene

Principal results: Site 1013 is located in San Nicolas Basin, within the middle band of basins of the California Borderland at a water depth of 1564 mbsl. The primary objective of drilling at this site was to sample a high-resolution section from the early Pliocene to Quaternary to study the evolution of the California Current system and to study oceanographic processes in intermediate waters as Northern Hemisphere glaciations expanded. Site 1013 will also provide information about organic carbon diagenesis and about minor element geochemistry through interstitial water profiles and through solid phase analyses.

Three holes were cored with the APC/XCB at Site 1013 to a maximum depth of 146.1 mbsf, which recovered uppermost Pliocene to Quaternary sediments (Fig. 1). Hole 1013A was cored with the APC to 90.6 mbsf and extended with the XCB to 146.1 mbsf. Hole 1013B was cored with the APC from 0 to 94.1 mbsf and extended with the XCB to 103.8 mbsf. Eight APC cores from 0 to 72.2 mbsf were recovered at Hole 1012C. Detailed comparisons of the three holes between the magnetic susceptibility generated on the MST and high-resolution color reflectance measured with the Oregon State University system demonstrated complete recovery of the sedimentary sequence down to 97 mbsf.

The sedimentary sequence recovered from the three holes at Site 1013 consists of an apparently continuous 146-m-thick interval of upper Pliocene (2.7 Ma) through Quaternary sediments. Sediments gradually change from fine-grained mixtures of siliciclastic and calcareous biogenic components to predominantly calcareous components. Sediments are interbedded on a sub-meter to several meters scale. Siliciclastic clay and silt are found throughout the cored interval but strongly decrease downhole. Calcareous nannofossils and, to a lesser extent, foraminifers, strongly increase with depth and dominate the calcareous fraction of the sediments. The biosiliceous component is negligible. Thin siliciclastic sand layers occur in the upper part of the sequence and distinct ash layers occur throughout the lower part of the sequence. Sedimentation rates throughout the section are around 65 m/m.y.

[1]Lyle, M., Koizumi, I., Richter, C., et al., 1997. *Proc. ODP, Init. Repts.*, 167: College Station, TX (Ocean Drilling Program).
[2]Shipboard Scientific Party is given in the list preceding the Table of Contents.

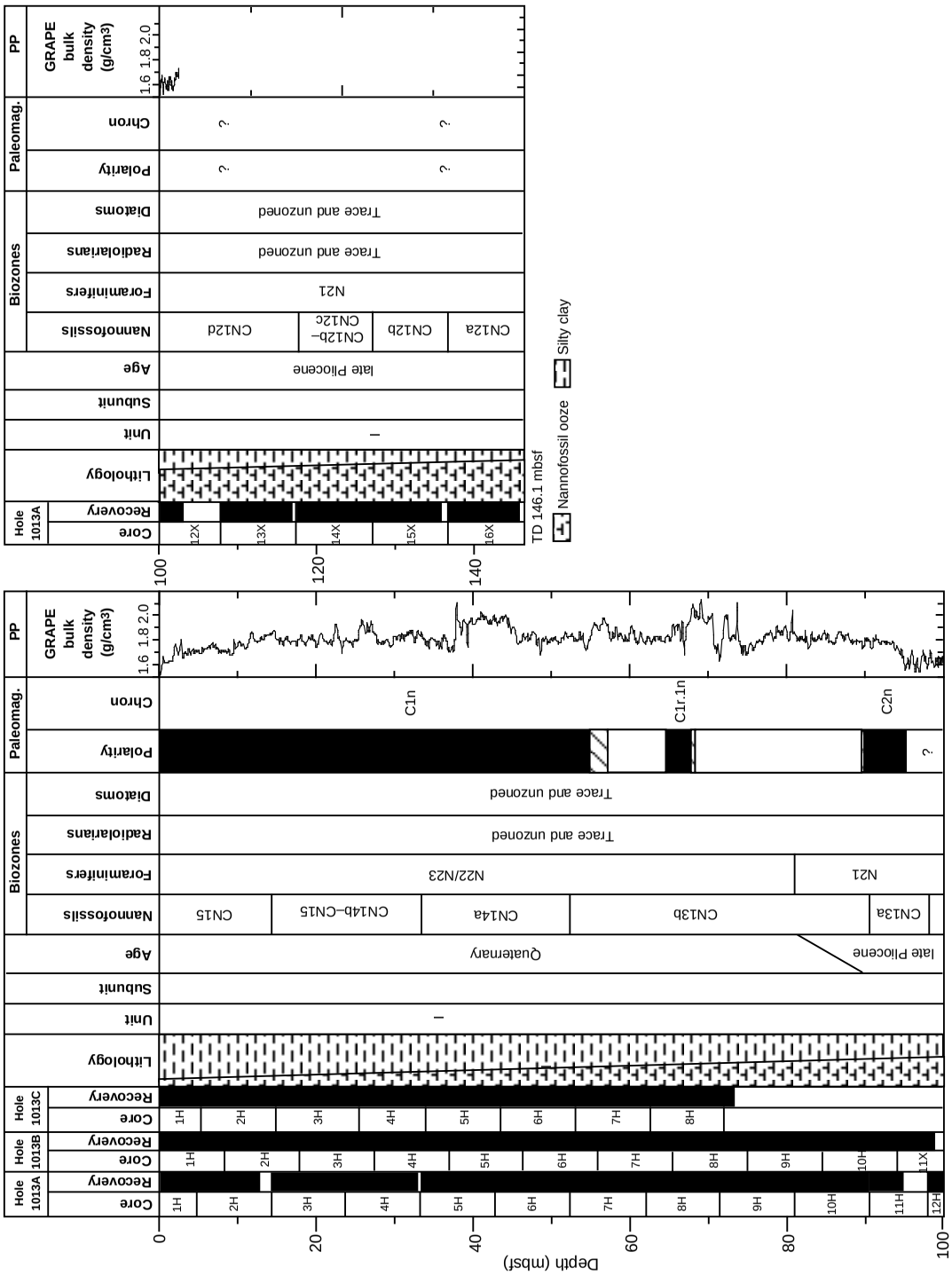

Figure 1. Site 1013 master column.

Biostratigraphic age control was provided by calcareous nannofossils and foraminifers. Radiolarians and diatoms are absent in the sequence except for conspicuous reworking of middle Miocene species. Latest Pliocene through Quaternary planktonic foraminifer assemblages indicate large-scale oscillations in sea-surface temperatures associated with glacial/interglacial episodes. Benthic foraminifer assemblages suggest relatively low oxygen concentrations in the basin during the late Neogene. Near suboxic to suboxic basinal conditions occurred during the latest Pliocene to earliest Quaternary.

Paleomagnetic investigations revealed a good magnetostratigraphic record down to 95 mbsf (Fig. 1) and allowed identification of the Brunhes, Jaramillo, Cobb Mountain (?), and the top of the Olduvai normal polarity intervals. Concentrations of biogenic hydrocarbon gases rapidly increase in the upper 20 mbsf and stay consistently high throughout the sedimentary column. The interstitial water geochemistry reflects the influence of organic carbon diagenesis by sulfate reduction, biogenic opal dissolution, and possible authigenic mineralization reactions. Nonconservative profiles of calcium and magnesium suggest the importance of authigenic mineralization. Organic carbon typically ranges between 1 and 6 wt% (max. 9 wt%). The ratios of total organic carbon to total nitrogen indicate a marine provenance for the organic matter at this site. Downhole temperature measurements yield a thermal gradient of 72°C/km and a heatflow estimate of 65 mW/m^2.

BACKGROUND AND OBJECTIVES

General Description

Site 1013 is located about 100 km west of San Diego, California, in San Nicolas Basin, within the third band of basins from the seaward edge of the California Borderland (see Fig. 4, in "Site 1012" chapter, this volume). Water depth at the drill site is shallow (1564 mbsl), and the sill depth for waters entering the deep basin is also shallow, 1106 mbsl (Emery, 1960). The site was surveyed in detail with the *Maurice Ewing* on cruise EW9504 in 1995 (Lyle et al., 1995a, 1995b; Fig. 2). Because of a major slump deposit along the western basin floor and because of an abandoned explosives dump near the center of San Nicolas Basin, the site was located on the southern flank. It is located in hemipelagic sediments slightly shallower than the turbidite fill in the basin center. Sedimentary bedding in the basin has small tight folds indicative of active compression. This is the only basin from the site survey that exhibited this folding. It was impossible to detect basement at this site from the seismic reflection profiles collected on EW9504. Sedimentary fill underneath Site 1013 is at least 1.3 s TWT thick, or probably more than a kilometer. The maximum drilling depth at Site 1013, in contrast, was only 150 mbsf.

Site Objectives

Site 1013 was drilled to sample a high-resolution section from the lower Pliocene to Quaternary in the San Nicolas Basin to study the evolution of the California Current system and to study oceanographic processes in intermediate waters as Northern Hemisphere glaciation expanded. Deep water within San Nicolas Basin enters primarily from the south, from sills connected to Animal Basin (Site 1011; Emery, 1960). Benthic foraminiferal isotope data at Site 1013 should therefore be conditioned by intermediate waters at the sill depth (1106 mbsl). The sill depth of the San Nicolas Basin approaches the modern depth of the oxygen minimum (~700 mbsl).

Site 1013 should also provide important new information about organic carbon diagenesis and about minor element geochemistry through interstitial water profiles and through solid phase analyses. Interstitial water sampling, especially within the upper 100 m, will be used to define organic matter diagenesis and oxidant removal from interstitial waters and sediments. Organic geochemical analyses will provide data on organic matter preservation in a low oxygen environment. Because of its location, away from the turbidites that fill the inner California Borderland basins, we expected that most of the organic matter in the basin to be marine in origin.

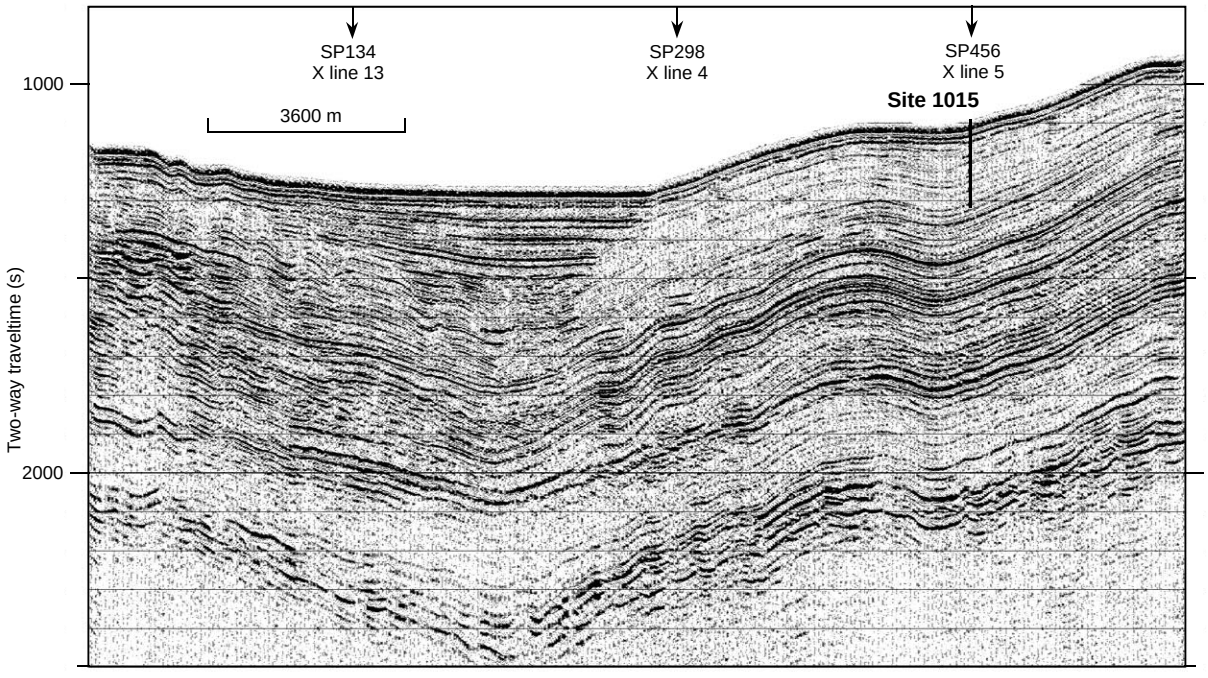

Figure 2. Seismic reflection profile through Site 1013 (Line EW9504 BA2-1; Lyle et al., 1995a, 1995b). San Nicolas Basin has a very thick sedimentary fill, and basement cannot be resolved by the seismic reflection survey. On y-axis, (s) = milliseconds.

OPERATIONS

Transit from Site 1012 to Site 1013

The 38.0-nmi transit from Site 1012 to Site 1013 was accomplished in 3.25 hr at an average speed of 11.7 kt. The *JOIDES Resolution* arrived at Site 1013 at 1345 hr on 5 May. A 3.5-kHz precision depth recorder (PDR) survey was performed while approaching Site 1013. A Datasonics 354M beacon was dropped on Global Positioning System coordinates at 1345 hr on 5 May.

Hole 1013A

Hole 1013A was spudded at 1730 hr on 5 May. APC Cores 167-1013A-1H through 10H were taken from 0 to 90.6 mbsf with 100.8% recovery (Table 1; see Table 2 on CD-ROM in the back pocket of this volume for a more detailed coring summary). Oriented cores were obtained starting with Core 167-1013A-3H. XCB Cores 167-1013A-11X through 16X were taken to 146.1 mbsf with 82.2% recovery.

Hole 1013B

Hole 1013B was spudded at 0730 hr on 6 May. APC Cores 167-1013B-1H through 10H were taken from 0 to 94.1 mbsf with 104.8% recovery (Table 1). XCB Core 167-1013B-11X was taken down to 103.8 mbsf with 96.8% recovery. Hole 1013B was originally scheduled to penetrate to 150 mbsf but was cut short due to the constraint of having to arrive in San Diego at 0500 hr on 7 May.

Hole 1013C

Hole 1013C was spudded at 1430 hr on 6 May. APC Cores 167-1013C-1H through 8H were taken down to 72.2 mbsf with 102.4% recovery (Table 1). Adara temperature measurements were taken on Cores 167-1013C-4H, 6H, and 8H (see "Physical Properties" chapter, this volume). The time allowed for Site 1013 expired and the drill string was tripped back to the surface and secured for the 8-hr transit to San Diego by 2115 hr 6 May.

LITHOSTRATIGRAPHY

Introduction

A 146.1-m-thick, continuous Quaternary to upper Pliocene (0.0–2.7 Ma) sedimentary sequence was recovered at Site 1013. Sediments gradually change downcore from mixtures of siliciclastic and calcareous biogenic components to predominantly calcareous composition (Fig. 3). Sediments of varied composition are interbedded on a scale of 50 to 250 cm throughout the section. Calcareous nannofossils and, to a lesser extent, foraminifers/carbonate grains dominate the calcareous fraction of the sediments. The siliceous component is negligible but consists of diatoms and/or sponge spicules. Thin terrigenous siliciclastic sand layers are intercalated in the upper part of the sequence. Volcanic glass is present and occurs disseminated throughout the dominant lithologies and as distinct ash layers, especially around 50 and 100 mbsf.

The sedimentation rate is relatively constant throughout the sequence (see "Biostratigraphy" section, this chapter), although calci-

Table 1. Coring summary for Site 1013.

Core	Date (May 1996)	Time	Top (mbsf)	Bottom (mbsf)	Length cored (m)	Length recovered (m)	Recovery (%)
167-1013A-							
1H	06	0035	0.0	5.1	5.1	5.10	100.0
2H	06	0100	5.1	14.6	9.5	7.64	80.4
3H	06	0200	14.6	24.1	9.5	10.17	107.0
4H	06	0225	24.1	33.6	9.5	9.10	95.8
5H	06	0250	33.6	43.1	9.5	9.86	104.0
6H	06	0315	43.1	52.6	9.5	9.93	104.0
7H	06	0400	52.6	62.1	9.5	9.91	104.0
8H	06	0435	62.1	71.6	9.5	9.93	104.0
9H	06	0515	71.6	81.1	9.5	10.52	110.7
10H	06	0600	81.1	90.6	9.5	9.32	98.1
11X	06	0800	90.6	98.1	7.5	4.22	56.2
12X	06	0855	98.1	107.7	9.6	4.83	50.3
13X	06	0945	107.7	117.3	9.6	8.98	93.5
14X	06	1035	117.3	126.9	9.6	9.64	100.4
15X	06	1115	126.9	136.5	9.6	8.98	93.5
16X	06	1230	136.5	146.1	9.6	8.97	93.4
167-1013B-							
1H	06	1440	0.0	8.6	8.6	8.64	100.0
2H	06	1505	8.6	18.1	9.5	10.03	105.6
3H	06	1530	18.1	27.6	9.5	9.72	102.0
4H	06	1550	27.6	37.1	9.5	10.09	106.2
5H	06	1620	37.1	46.6	9.5	10.07	106.0
6H	06	1645	46.6	56.1	9.5	10.09	106.2
7H	06	1720	56.1	65.6	9.5	9.97	105.0
8H	06	1755	65.6	75.1	9.5	10.28	108.2
9H	06	1830	75.1	84.6	9.5	10.10	106.3
10H	06	1910	84.6	94.1	9.5	9.59	101.0
11X	06	2015	94.1	103.8	9.7	9.39	96.8
167-1013C-							
1H	06	2140	0.0	5.7	5.7	5.69	99.8
2H	06	2200	5.7	15.2	9.5	9.87	104.0
3H	06	2220	15.2	24.7	9.5	9.97	105.0
4H	06	2300	24.7	34.2	9.5	9.48	99.8
5H	06	2330	34.2	43.7	9.5	9.71	102.0
6H	07	0005	43.7	53.2	9.5	9.87	104.0
7H	07	0035	53.2	62.7	9.5	9.80	103.0
8H	07	0100	62.7	72.2	9.5	9.57	101.0

Note: Table 2, on CD-ROM, back pocket, this volume, is a more detailed coring summary.

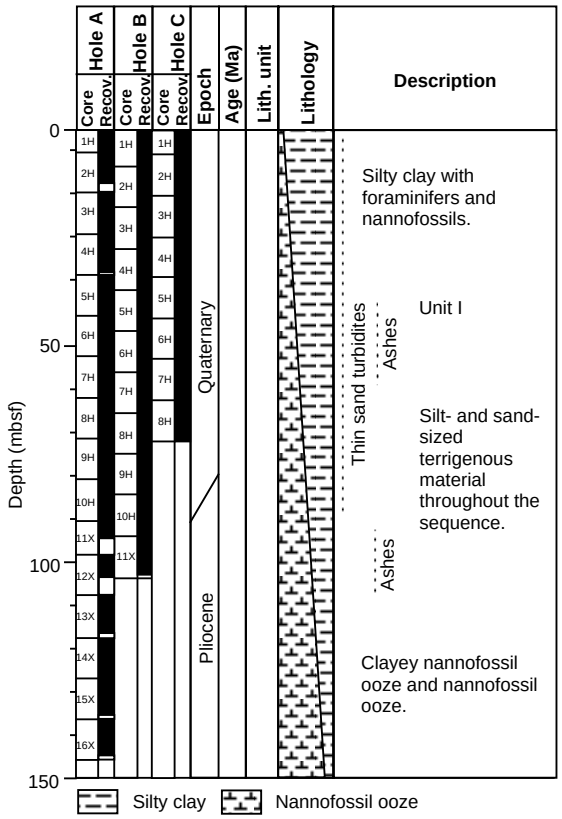

Figure 3. Site 1013 lithostratigraphic summary (0–150 mbsf).

um carbonate content increases gradually downhole (see "Organic Geochemistry" section, this chapter, and smear-slide descriptions) without any sharp lithologic changes. The sediments are consequently assigned to one lithostratigraphic unit without subdivisions.

Description of Units

Unit I

Hole 1013A, interval 167-1013A-1H-1 through 16X; 0–146.1 mbsf (base of hole);
Hole 1013B, interval 167-1013B-1H-1 through 11X; 0–103.8 mbsf (base of hole);
Hole 1013C, interval 167-1013C-1H-1 through 8H; 0–72.2 mbsf (base of hole).
Age: Quaternary to latest Pliocene, 0.0–2.7 Ma.

Unit I is predominantly composed of dark grayish brown (2.5Y 3/1 to 5Y 3/1) to dark olive gray (5Y 3/2) silty clay with foraminifers and nannofossils, and dark olive gray (5Y 3/2) to olive gray (5Y 4/2, 5Y 5/3) clayey nannofossil ooze to nannofossil ooze. The former lithology is gradually replaced downward by the latter. Sediments are interbedded at two scales: ~50 cm and 200–250 cm and are slightly to moderately bioturbated throughout the section. Clay content (based on smear-slide observations) varies from 5% to 80% (average 40%). The silt component consists mainly of feldspar (0% to 20%), quartz (0% to 15%), nannofossils (0%–80%, average 40%), fresh and altered volcanic glass fragments (0% to 5%, average 15%), and varying but minor components of diatoms, radiolarians, and sponge spicules. Most prominent in the sand component are foraminifers (0%–35%) and carbonate grains (0%–20%), which both increase gradually with depth.

Thin dark olive gray (5Y 3/2) graded sand layers (containing quartz, feldspar, and/or foraminifers) and thin white to light gray (N7) vitric ash layers are scattered throughout the section. These are most common in the upper part of the section but are still present only as minor lithologies.

Depositional History

The sedimentary sequence at Site 1013 records a gradual shift from calcareous to siliciclastic sedimentation from the late Pliocene to the present. Alternation of siliciclastic clay and nannofossil ooze accumulated at a relatively constant sedimentation rate of approximately 50 m/m.y. The compositional and color alternations reflect cyclic variations with ~10 k.y. and 40–50 k.y. periodicity.

Deposition of volcanic ash was clustered in two distinct intervals of the Quaternary and Pliocene. Thin graded sand layers, interpreted as turbidites, occurred principally in the Quaternary, in conjunction with the overall increase in siliciclastic material. The quartz, feldspar, and foraminifers of the turbidites likely have their origin on nearby bathymetric highs.

Site 1013 was otherwise isolated from major clastic sources. Nevertheless, the sedimentation rate is high, reflecting the decreasing accumulation of calcareous (and siliceous) organisms paralleled by increasing siliciclastic deposition through time.

BIOSTRATIGRAPHY

The sedimentary sequence recovered from the three holes at Site 1013 consists of an apparently continuous 146-m-thick interval of upper upper Pliocene (2.7 Ma) through Quaternary sediments. Calcareous nannofossils are abundant throughout and preservation is moderate to good. Planktonic foraminifers are abundant and well preserved in the Quaternary; they are abundant to rare and moderately well preserved in the latest Pliocene. Radiolarians and diatoms are absent in the sequence except for conspicuous reworking of middle Miocene species. Reworked calcareous nannofossils of middle Miocene and Eocene age occur in the Quaternary. Planktonic foraminifers show little evidence of reworking.

A well-constrained biostratigraphy and chronology for Hole 1013A is provided by calcareous nannofossil and planktonic foraminifer datums for the upper part of the Pliocene and Quaternary. An age/depth plot for Hole 1013A (Fig. 4) shows continuous sedimentation from the upper Pliocene (2.7 Ma) to the Quaternary.

Latest Pliocene through Quaternary planktonic foraminifer assemblages indicate large-scale oscillations in sea-surface tempera-

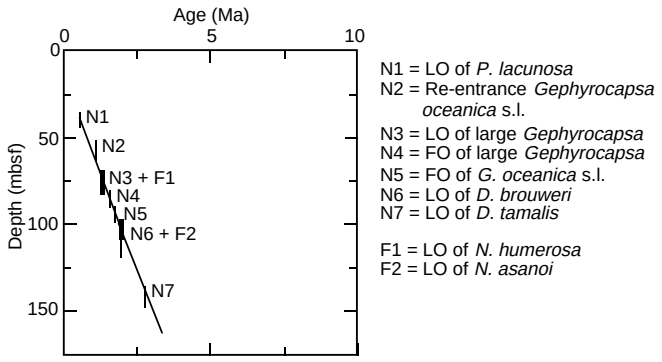

Figure 4. Age/depth plot for Hole 1013A. LO = last occurrence, FO = first occurrence.

tures associated with glacial/interglacial episodes. Benthic foraminifer assemblages suggest relatively low oxygen concentrations in the basin during the late Neogene. Near suboxic to suboxic basinal conditions occurred during the latest Pliocene to earliest Quaternary.

Planktonic Foraminifers

Site 1013 contains a continuous planktonic foraminifer sequence ranging from the latest Pliocene (2.5 Ma) to the Quaternary (Table 3). Foraminifers are highly abundant and very well preserved in the Quaternary and are abundant to rare and moderately well preserved in the latest Pliocene. Specimen fragmentation is common in the Pliocene assemblages, with the coarse fraction larger than 250 µm often dominated by robust forms. This report is based on observation and tabulation of species and assemblages from core-catchers of Hole 1013A (Table 3). Biostratigraphy of planktonic foraminifers is similar to that of the late Pliocene to Quaternary of Site 1012. As in Site 1012, the Quaternary at Site 1013 is of special interest because of the quality of preservation of foraminifers, the relative thickness of the sequence, and because of evidence of faunal changes that reflect oscillations between glacial and interglacial episodes.

The sequence of biostratigraphic changes is similar to the late Pliocene and Quaternary of Site 1012. The base of the Quaternary at Site 1013 is not clearly marked because of the absence of *Globorotalia truncatulinoides.* The Quaternary/Pliocene boundary (between Samples 167-1013A-10H-CC and 9H-CC) is placed within the upper range of *Neogloboquadrina humerosa* and before the LO of *Neogloboquadrina asanoi.*

The LO of *N. asanoi* at 1.9 Ma occurs at 107 mbsf (Sample 167-1013A-12H-CC). The LOs of *Neogloboquadrina* sp. ("rounded") and *Globorotalia puncticulata* occur in the same stratigraphic order as at Site 1012.

The only notable difference between the planktonic foraminifer sequence at Site 1013 and Site 1012 is that *Neogloboquadrina pachyderma* (sinistral) occurs in abundance in the latest Pliocene rather than in the Quaternary at Site 1012. The earlier appearance of this species at Site 1013 is probably caused by the more northern, cooler location of the sequence.

Benthic foraminifers are abundant, diverse, and extremely well preserved throughout the entire Quaternary of Site 1013. *Uvigerina* is generally abundant to common throughout. Other taxa often present include *Globobulimina, Bolivina, Bulimina, Hoeglundina, Gyroidina, Cassidulina, Epistominella,* and *Cibicidoides.* The associations are indicative of relatively low oxygen concentrations in the basinal deep waters throughout much of the sequence. *Bolivina* is an important element in the benthic foraminifer assemblages in the earliest Quaternary and latest Pliocene between 72 mbsf and 117 mbsf (between Samples 167-1013A-8H-CC and 13X-CC). The abundance of *Bolivina* in this interval suggests even lower oxygen concentrations at this time in bottom waters. The benthic foraminiferal assemblages indicate lower levels of basinal oxygen during the late Neogene than in the East Cortes Basin Site 1012.

Calcareous Nannofossils

Nannofossils are generally common to abundant and well preserved in the upper Pleistocene and upper Pliocene sections of Site 1013 (Table 4). In the lower Pleistocene, the preservation is moderate. Calcareous nannofossil assemblages recovered at Site 1013 are similar to those of Site 1012. The important difference between the assemblages of both sites is the strong reworking of Miocene and Eocene floras in Quaternary assemblages of Site 1013. An interval spanning the lower upper Pliocene Zone CN12a to the upper Pleistocene Zone CN 15 was recognized in Hole 1013A. Hole 1013B represents an interval ranging from the upper upper Pliocene Zone CN13a to the upper Pleistocene Zone CN15. Hole 1013C is a sequence of Pleistocene age (Zones CN15 to CN13b).

Pleistocene nannofossil assemblages are marked by the presence of *Emiliania huxleyi, Pseudoemiliania lacunosa, Calcidiscus leptoporus, Helicosphaera carteri, Helicosphaera sellii,* and several morphotypes of *Gephyrocapsa* spp. and *Ceratolithoides.* The expanded Quaternary sequence allowed us to recognize the re-entrance of *Ge-*

Table 3. Distribution and relative abundances of planktonic foraminifers in Hole 1013A.

Zone	Core, section, interval	Depth (mbsf)	Abundance	Preservation	*Neogloboquadrina dutertrei*	*Globorotalia inflata*	*Globorotalia puncticulata*	*Globorotalia crassaformis*	*Neogloboquadrina asanoi*	*Neogloboquadrina* sp. "rounded"	*Sphaeroidinella dehiscens*	*Neogloboquadrina pachyderma* dex.	*Neogloboquadrina pachyderma* sin.	*Globigerina bulloides*	*Orbulina universa*	*Globigerinoides ruber*	*Globorotalia tumida*	*Globoratoloides hexagona*	*Globorotalia scitula*	*Globigerinita glutinata*	*Globigerina quinqueloba*	*Globigerina apertura*	*Globorotalia hirsuta*
	167-1013A-																						
	1H-CC	5.1	A	G									A	A	C			R	R		A		
	2H-CC	14.6																					
	3H-CC	24.1	A	G		R							A	A									
	4H-CC	34.0																					
N22/23	5H-CC	43.0	A	G									A	A						R			R
	6H-CC	53.0	A	G		F						A		A	F	R				F	A		
	7H-CC	62.0	A	G	A	F		F				A	A	A							A		F
	8H-CC	72.0	A	G				F					A	A	F								F
	9H-CC	81.0	A	M		A		F					A	A	C	R		R					
	10H-CC	91.0	R	M								R		R									
	11H-CC	98.0	C	M								F	A	A							A	R	
	12H-CC	107.0	C	M					A				A	A	R						C		
N21	13H-CC	117.0	A	G				R	A				A	A		R					C	R	
	14X-CC	127.0	A	M					A	A				A									
	15X-CC	136.0	C	M					A	F	R	A	F	A									
	16X-CC	146.0	F	M		F	F		A					A	R		F						

Note: See "Explanatory Notes" chapter for abbreviations.

Table 4. Distribution and relative abundances of calcareous nannofossils at Site 1013.

Zone	Core, section, interval (cm)	Depth (mbsf)	Preservation	Abundance	*Emiliania huxleyi*	*Pseudoemiliania lacunosa*	*Helicosphaera carteri*	*Helicosphaera sellii*	*Gephyrocapsa oceanica* s.l.	*Gephyrocapsa* sp. 3	*Gephyrocapsa* small	*Gephyrocapsa* large	*Discoaster brouweri*	*Discoaster triradiatus*	*Discoaster pentaradiatus*	*Discoaster surculus*	*Discoaster tamalis*	*Reticulofenestra pseudoumbilicus*	*Ceratholithus* spp.	*Coccolithus pelagicus*	*Calcidiscus macintyrei* >11 µm	*Calcidiscus premacintyrei*	*Calcidiscus leptoporus*	*Cyclicargolithus floridanus*	Reworked
	167-1013A-																								
CN15	1H-CC	5.1	G	A	P		C			F	A									P					F
CN15	2H-6, 7	14.6	G	A	P				C		A									F			R		
CN15–CN14b	3H-CC	24.1	G	A					C		A														T
CN15–CN14b	4H-7, 54	33.6	G	A			F		P		A									F					
CN14a	5H-CC	43.1	M	A		C/F	C		R	R	C/A							F/C		C		R/F		C	C
CN14a	6H-CC	52.6	G	A		P	P		P	R/F	D							P					R		F
CN13b?	7H-CC	62.1	G	A		C					A							P					F		F
CN13b?	8H-CC	71.6	M/G	A		C	R				A									C			F		F
CN13b	9H-CC	81.1	P/M	C		C	C	R				F/R											C		F/C
CN13b	10H-CC	90.6	P	R/F		P			P														R		
CN13a	11H-CC	98.1	P	C		P	P														C				T
CN12d?	12H-CC	107.7	G	A									R							C	C				
CN12d	13X-CC	117.7	G	A		C							F							R	C		P		
CN12c–CN12b	14X-CC	126.9	G/M	A		P							F		F	F					C		P		
CN12b	15X-CC	136.5	G	A										R	C	C				P	R		R		
CN12a	16X-CC	146.1	G	A		R	P	R							P	P	P		R						
	167-1013B-																								
CN15	1H-CC	8.6	P	F	P	R			R																
	2H-CC	18.1		B																					
CN15–CN14b	3H-CC	27.6	G	A			F		C											F/C			R		
CN14a	4H-CC	37.1	G	A		F	R		P		A	RR											P		
CN14a	5H-CC	46.6	P	RR		P																			
CN14a	6H-CC	56.1	G	A			C		P	C	D												C		
CN13b	7H-CC	65.6	M/G	A		C	R				A								R	F			P		
CN13b	8H-CC	75.1	G	A		C						P											R		
CN13b	9H-CC	84.6	M	A		C	R	R	P		A									F			C		
CN13b	10H-CC	94.1	P	F		P		R	R												P		P		
CN13a	11X-CC	103.0	P/M	C		C															C		C		
	167-1013C-																								
CN15	1H-CC	5.7	G	A	P		C	R	C		A	F											R		
CN15–CN14b	2H-CC	15.2	P	R			R		R		P												R		F
CN15–CN14b	3H-CC	24.7	G	A					P		A									F			R		
CN15–CN14	4H-CC	34.2	G	A		R			P		A									F			R		T
CN14a	5H-CC	43.7	G	A		C	R		R/F	F	A														
CN13b	6H-CC	53.2	M	R		P	R				P												R		
CN13b	7H-CC	62.7	M	C/A		P					C												P		
CN13b	8H-CC	72.2	M	F		C						C													

Note: See "Explanatory Notes" chapter for abbreviations.

phyrocapsa oceanica s.l., the LO and FO of large *Gephyrocapsa,* and the FO of *G. oceanica* s.l.

The Pliocene/Pleistocene boundary is placed between Samples 167-1013A-10H-CC and 11H-CC by the FO of *G. oceanica* s.l.

Pliocene nannofossil assemblages are marked by an association of *H. carteri, Discoaster brouweri, D. tamalis, D. pentaradiatus, D. surculus,* and several morphotypes of *Reticulofenestra* and *Ceratolithus*. The LO of *D. brouweri* (base of Zone CN13a) and the LO of *D. tamalis* (base of Zone CN12b) were recognized in Samples 167-1013A-12H-CC and 16X-CC, respectively.

Diatoms

Diatoms are barren to few in all sections from the Pliocene through Quaternary interval at Site 1013. Assemblages are very poorly preserved, and are similar to those of Site 1012. No correlation with the Leg 167 North Pacific diatom zonation can be made (Table 5).

Biosiliceous mixtures composed of reworked planktonic diatoms and radiolarians, mostly of middle Miocene age, and fresh sponge spicules are persistently scattered throughout all core catchers. The diatoms are commonly dissolved and fragmented, which is indicative of a persistent and strong reworking of pelagic middle Miocene deposits, whereas robust siliceous sponge spicules, which are resistant to transportation, suggest a continuous input of shallower coastal material during the accumulation of the Pliocene–Pleistocene deposits at this site.

PALEOMAGNETISM

Laboratory Procedures

We made magnetic measurements using the pass-through cryogenic magnetometer on the archive halves of 10 APC cores and one XCB core from Hole 1013A, and on the working halves of four APC cores from Hole 1013C. Based on the results after alternating field (AF) demagnetization at 20 or 25 mT, there is a good magnetostratigraphic record above 95 mbsf.

A downhole record of the intensity and inclination of natural remanent magnetization (NRM) before and after AF demagnetization is shown for Hole 1013A in Figure 5. Alternating field demagnetization at 20 mT removes a large fraction of the drilling-induced magnetization. The NRM between 55 and 90 mbsf with normal polarity before AF demagnetization is reversely magnetized after AF treatment. In the depth interval between 38 and 72 mbsf in Hole 1013C,

Table 5. Distribution and relative abundances of diatoms at Site 1013.

Core, section, interval	Depth (mbsf)	Abundance	Preservation	Diatom fragments	*Actinocyclus ingens*	*Actinocyclus ingens nodus*	*Actinocyclus oculatus*	*Actinocyclus tsugaruensis*	*Coscinodiscus marginatus*	*Coscinodiscus marginatus fossilis*	*Coscinodiscus* sp.	*Crucidenticula nicobarica*	*Denticulopsis hustedtii*	*Denticulopsis hyalina*	*Denticulopsis lauta*	*Denticulopsis lauta* s.l.	*Hemiaulus polymorphus*	*Neodenticula seminae*	*Stephanopyxis turris*	*Synedra jouseana*	*Synedra* sp.	*Thalassionema nitzschioides*	*Thalassionema schraderi*	*Thalassiothrix longissima*	Sponge spicules
167-1013A-																									
1H-CC	5.1	T	P	P														P				P			P
3H-CC	24.1	T	P	P									P	P											P
5H-CC	43.1	C	P/M				P		P			P		P	P		P		P	P				P	
6H-CC	52.6	T	P	P	P	P							P									P				P
7H-CC	62.1	T	P	P	P											P										P
8H-CC	71.6	T	P	P	P									P												P
9H-CC	81.1	T	P	P					P													P				P
10H-CC	90.6	T	P		P														P							P
11X-CC	98.1	R	P/M	P	P				P																	P
12X-CC	107.7	T	P						P					P												P
13X-CC	117.7	R	P	P	P	P			P					P							P					P
14X-CC	126.9	F	P		P			P	P	P												P				P
15X-CC	136.5	R	P						P	P				P												C
16X-CC	146.1	R	P		P				P		P		P	P									P			C
167-1013B-																										
1H-CC	8.6	R	P	P	P				P										P							F

Notes: P = present; more detailed abundance information not available. See "Explanatory Notes" chapter for other abbreviations.

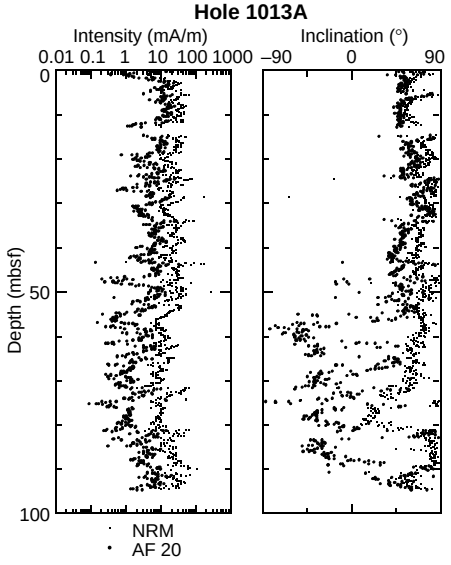

Figure 5. Plots of magnetic intensity (left) and inclination (right) of cores from Hole 1013A. Small and large dots represent magnetic intensity and inclination before and after AF demagnetization at 20 mT, respectively.

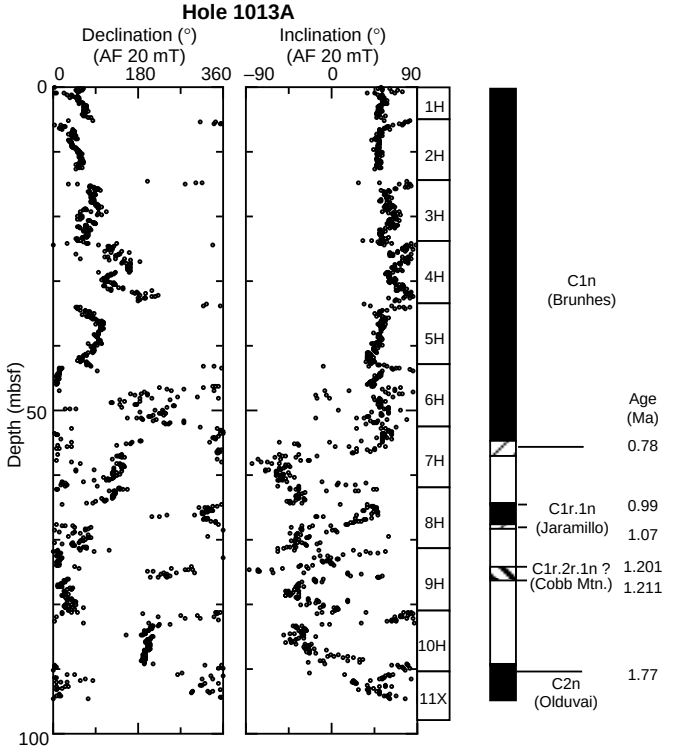

Figure 6. Plots of declination and inclination data from Hole 1013A after 20 mT AF demagnetization with the magnetostratigraphic polarity interpretation. The ages of the reversal boundaries are from Cande and Kent (1995).

the remanent magnetization was measured before and after AF demagnetization at 25 mT for comparison with the magnetic reversal horizons determined in Hole 1013A (Figs. 6, 7). We identified normal and reversed polarity chrons based on the polarity of the inclination.

Results and Discussion

The interpretation of the inclination record after AF demagnetization in Holes 1013A and 1013C in terms of geomagnetic polarity chrons is shown in Figures 6 and 7, respectively. The reversal boundaries with their depths and associated ages are summarized in Table 6. The magnetic polarity boundaries occur in the two holes at the same horizons as correlated by measurements of whole-core magnetic susceptibility (see "Composite Depths and Sedimentation Rates" section, this chapter).

Chron C1n (Brunhes) extends from the top of the core to 55 mbsf in Hole 1013A and 1013C. A few measurements of the inclination in Core 167-1013A-6H gave negative values. These anomalous mag-

netic directions are probably caused by core disturbance. The Jaramillo subchronozone (C1r.1n) occurs over an interval of about 4 m in Hole 1013A. The top of the Jaramillo cannot be determined in Hole 1013C, because of coring disturbance at the top of Core 167-1013C-8H. The bottom (onset) of the Jaramillo is well defined in both holes between 68 and 69 mbsf (Table 6). Positive inclinations, together with a large change in declination, are found in Core 167-1013A-9H at about 76 mbsf, which can be assigned to the Cobb Mountain cryptochron. The bottom of Core 167-1013A-10H and all of Core 11X are most likely normally magnetized despite some scatter in the inclinations. This normal interval below 89 mbsf is correlated to the Olduvai (C2n) chronozone in agreement with biostratigraphic results (see "Biostratigraphy" section, this chapter).

In summary, a comparison of the downhole inclination plots from Holes 1013A and 1013C (Figs. 6, 7) shows similar features in both records, confirming the complete magnetostratigraphic interpretation in Figure 6. An age/depth plot of the magnetostratigraphic datums in Hole 1013A, based on the time scale of Cande and Kent (1995), is shown in Figure 8. The high sedimentation rate of about 65 m/m.y. around the Jaramillo magnetozone decreases below the Cobb Mountain cryptochron.

COMPOSITE DEPTHS AND SEDIMENTATION RATES

Multisensor track (MST) data collected at 4-cm intervals from Holes 1013A through 1013C and color reflectance data collected at 6- to 10-cm intervals from Holes 1013A through 1013C were used to determine depth offsets in the composite section. On the composite depth scale (expressed as mcd, meters composite depth), features of the plotted MST and color reflectance data in adjacent holes are aligned so that they occur at approximately the same depth. Working from the top of the sedimentary sequence, a constant was added to the mbsf (meters below seafloor) depth for each core in each hole to arrive at a mcd depth for that core. The depths offsets that compose the composite depth section are given in Table 7 (also on CD-ROM, back pocket). Continuity of the sedimentary sequence was documented only for the upper 97 mcd, and between 98 and 110 mcd. There are gaps in the sedimentary sequence at 97 mcd, and between cores below 110 mcd in Hole 1013A.

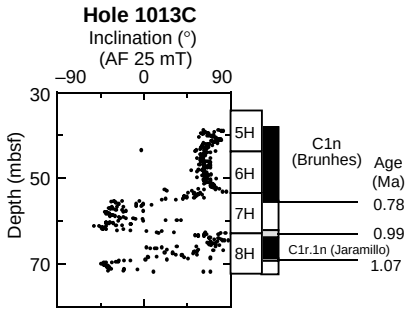

Figure 7. Inclination data from a selected depth interval of Hole 1013C after 25 mT. The magnetostratigraphic polarity interpretation confirms the reversal stratigraphy of Hole 1013A in Figure 6.

Magnetic susceptibility and color reflectance measurements were the primary parameters used for interhole correlation purposes. GRAPE bulk density measurements were not useful for interhole correlations because gas expansion in the cores severely affected the high-resolution bulk density trends. Natural gamma-ray activity measurements were made throughout the entire section in Holes 1013A through 1013C, but the sampling interval of 12 cm was insufficient for interhole correlation.

The magnetic susceptibility and color reflectance records used to verify core overlap for Site 1013 are shown on a composite depth scale in Figure 9. The GRAPE bulk-density data were used to identify intervals of voids and highly disturbed sediments (values less than 1.4 g/cm^3), and these intervals were culled from all the data (Fig. 9). The cores from Holes 1013A, 1013B, and 1013C provide continuous overlap to ~97 mcd. The composite records suggest that up to 2 m of material may be missing between cores down to about 110 mcd, although the average gap is less than 1 m. As there are no data to fill possible core gaps below 110 mcd, an assessment of core gap length below this depth is not possible.

Following construction of the composite depth section for Site 1013, a single spliced record was assembled from the aligned cores. Hole 1013B was used as the backbone of the sampling splice. Hole 1013A was primarily used to splice across core gaps in Hole 1013B. One core from Hole 1013C (Core 167-1013C-7H) was used in the splice because it contains a clear magnetic reversal. The composite depths were aligned so that tie points between adjacent holes occurred at exactly the same depths in meters composite depth. Intervals having significant disturbance or distortion were avoided if possible. The Site 1013 splice (Table 8, also on CD-ROM, back pocket) can be used as a sampling guide to recover a single continuous sedimentary sequence between 0–97 mcd and 98–110 mcd. Below 110 mcd the spliced record consists only of cores from Hole 1013A appended to each other because Holes 1013B and 1013C did not penetrate to that depth.

A preliminary age model (Table 9) was constructed to estimate sedimentation rates (Fig. 10). The age model was applied to the spliced records of GRAPE, magnetic susceptibility, and color reflectance shown in Figure 11.

INORGANIC GEOCHEMISTRY

We collected nine interstitial water samples from Hole 1013A at depths ranging from 2.95 to 131.35 mbsf. Chemical gradients in the

Table 6. Magnetostratigraphic datum levels in Holes 1013A and 1013B.

		Upper limit			Lower limit		
Chronozone boundary	Age (Ma)	Core, section	Level (cm)	Depth (mbsf)	Core, section	Level (cm)	Depth (mbsf)
		167-1013A-			167-1013A-		
C1n Brunhes (o)	0.780	7H-2	45	54.55	7H-3	125	56.85
C1r.1n Jaramillo (t)	0.990	8H-2	85	64.45	8H-2	10	564.65
C1r.1n Jaramillo (o)	1.070	8H-4	95	67.55	8H-5	5	68.15
C1r.2r.1n Cobb Mtn. (t)	1.201	9H-2	105	74.15			
C1r.2r.1n Cobb Mtn. (o)	1.211				9H-4	5	76.15
C2n Olduvai (t)	1.770	10H-6	45	89.05	10H-6	85	89.45
		167-1013C-			167-1013C-		
C1n Brunhes (o)	0.780	7H-2	35	55.05	7H-2	55	55.25
C1r.1n Jaramillo (o)	1.070	8H-4	125	68.45	8H-5	45	69.15

Notes: o = onset; t = termination; the assigned ages of the reversal boundaries are according to the time scale of Cande and Kent (1995). The upper and lower limits define the range within which a reversal occurs.

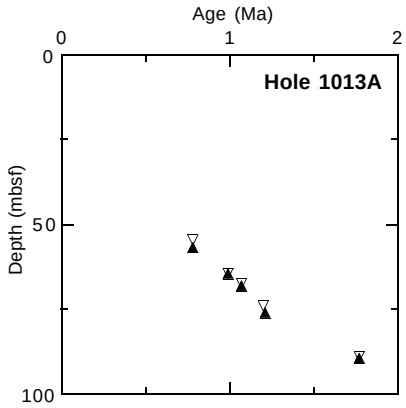

Figure 8. Age/depth plot for Hole 1013A. Open and solid triangles show the upper and lower limits of the magnetostratigraphic reversal boundaries. The sedimentation rate seems to slow between 75 and 95 mbsf.

Table 7. Site 1013 composite depth section.

Core, section	Depth (mbsf)	Offset (m)	Depth (mcd)
167-1013A-			
1H-1	0.00	0.00	0.00
2H-1	5.11	–0.10	5.01
3H-1	14.61	–0.28	14.33
4H-1	24.11	0.24	24.35
5H-1	33.61	0.42	34.03
6H-1	43.11	0.82	43.93
7H-1	52.61	0.94	53.55
8H-1	62.11	1.42	63.53
9H-1	71.61	1.87	73.48
10H-1	81.11	3.19	84.30
11X-1	90.61	2.36	92.97
12X-1	98.11	6.70	104.81
13X-1	107.71	6.70	114.41
14X-1	117.71	6.70	124.41
15X-1	126.91	6.70	133.61
16X-1	136.51	6.70	143.21
167-1013B-			
1H-1	0.01	0.00	0.01
2H-1	8.61	–0.40	8.21
3H-1	18.11	–0.01	18.10
4H-1	27.61	0.18	27.79
5H-1	37.11	0.18	37.29
6H-1	46.61	0.56	47.17
7H-1	56.11	0.71	56.82
8H-1	65.61	1.41	67.02
9H-1	75.11	2.87	77.98
10H-1	84.61	3.48	88.09
11X-1	94.11	3.48	97.59
167-1013C-			
1H-1	0.01	0.00	0.01
2H-1	5.71	0.04	5.75
3H-1	15.21	0.73	15.94
4H-1	24.71	0.44	25.15
5H-1	34.21	1.32	35.53
6H-1	43.71	1.76	45.47
7H-1	53.21	2.64	55.85
8H-1	62.71	3.32	66.03

Note: This table is also on CD-ROM, back pocket, this volume.

interstitial waters at this site (Table 10) reflect organic matter diagenesis via sulfate reduction, the dissolution of biogenic opal, and the influence of authigenic mineral precipitation.

Chlorinity increases by 4% from 2.95 to 9.55 mbsf, with concentrations in the deeper samples within the range of 554–572 mM (Fig. 12). Salinity, measured refractively as total dissolved solids, generally ranges from 34 to 36. Sodium concentrations measured by flame emission spectrophotometry were on average <2% lower than those estimated by charge balance (Table 10).

Alkalinity increases to values >50 mM by 46.05 mbsf (Fig. 12). Sulfate concentrations decrease rapidly in the uppermost sediments to values below the detection limit (approximately 1 mM) by 27.05 mbsf. Phosphate concentrations increase to a peak value >170 µM at 19.05 mbsf, then generally decrease with increasing depth, at first steeply, then more gradually, to 59 µM in the deepest sample at 131.35 mbsf. Ammonium concentrations increase with increasing depth to values greater than 13 mM in the deepest sample at 131.35 mbsf. Dissolved manganese concentrations were greater than the detection limit of 3 µM only in the shallowest sample, with a concentration of 4.2 µM at 2.95 mbsf.

Dissolved silicate concentrations increase with depth to values >1000 µM by 76.05 mbsf (Fig. 12), indicative of the dissolution of biogenic opal. Strontium concentrations increase with depth to >200 µM by 101.05 mbsf.

Calcium concentrations decrease to 3.5 mM at 38.05 mbsf, then increase with increasing depth to 6.4 mM in the deepest sample at 131.35 mbsf (Fig. 12). Magnesium concentrations decrease to 44.8 mM at 76.05 mbsf, then increase to an average of 49 mM in the two deepest samples from 101.05 to 131.35 mbsf. The decrease in dissolved calcium in the upper sediment and the nonlinear relationship of calcium and magnesium suggest that authigenic mineral precipitation is significant in influencing these profiles. Lithium concentrations increase with depth to 150 µM at 131.35 mbsf (Fig. 12).

ORGANIC GEOCHEMISTRY

We conducted measurements of elemental composition and volatile hydrocarbons in sediments from Site 1013 (for methods see "Organic Geochemistry" section, "Explanatory Notes" chapter, this volume).

Volatile Hydrocarbons

Because of shipboard safety and pollution prevention considerations, the concentrations of methane, ethane, and propane were routinely monitored in Hole 1013A. The results are displayed in Figure 13 and Table 11. Headspace methane concentration increases rapidly to 34,000 ppm at 38 mbsf. Below this level, the concentration decreases gradually with little fluctuation to values of ~9,000 ppm. Methane/ethane ratios show a gradual decrease from top to bottom of the hole. No significant amounts of higher molecular weight hydrocarbons were observed, indicating that the methane was derived from biogenic degradation of organic matter and is not significant for safety and pollution investigations. Whenever gas voids occurred, vacutainer samples were taken. Because of the direct gas sampling method, the values of the vacutainer samples are higher, but show the same pattern as the headspace samples.

Elemental Analysis

At Site 1013, 94 sediment samples were analyzed for total carbon, inorganic carbon, total nitrogen, and total sulfur. Results are presented in Table 12 (also on CD-ROM, back pocket) and Figure 14.

The percentage of calcium carbonate ($CaCO_3$) was calculated from the inorganic carbon concentrations by assuming that all carbonate occurs in the form of calcite. Average values of $CaCO_3$ concentration increase from the top (~15%) to the bottom (~45%) of Hole 1013A. Throughout the section, $CaCO_3$ concentration shows high amplitude fluctuations with a 7–20 m wavelength. These cycles may reflect the productivity of calcareous organisms, because the site is too shallow to be affected by changes in the calcium carbonate compensation depth (CCD).

The organic carbon record is characterized by high concentrations between 1.1 and 9.2 wt% throughout the sequence (Table 12; Fig. 14). In general, total organic carbon (TOC) contents decrease slightly

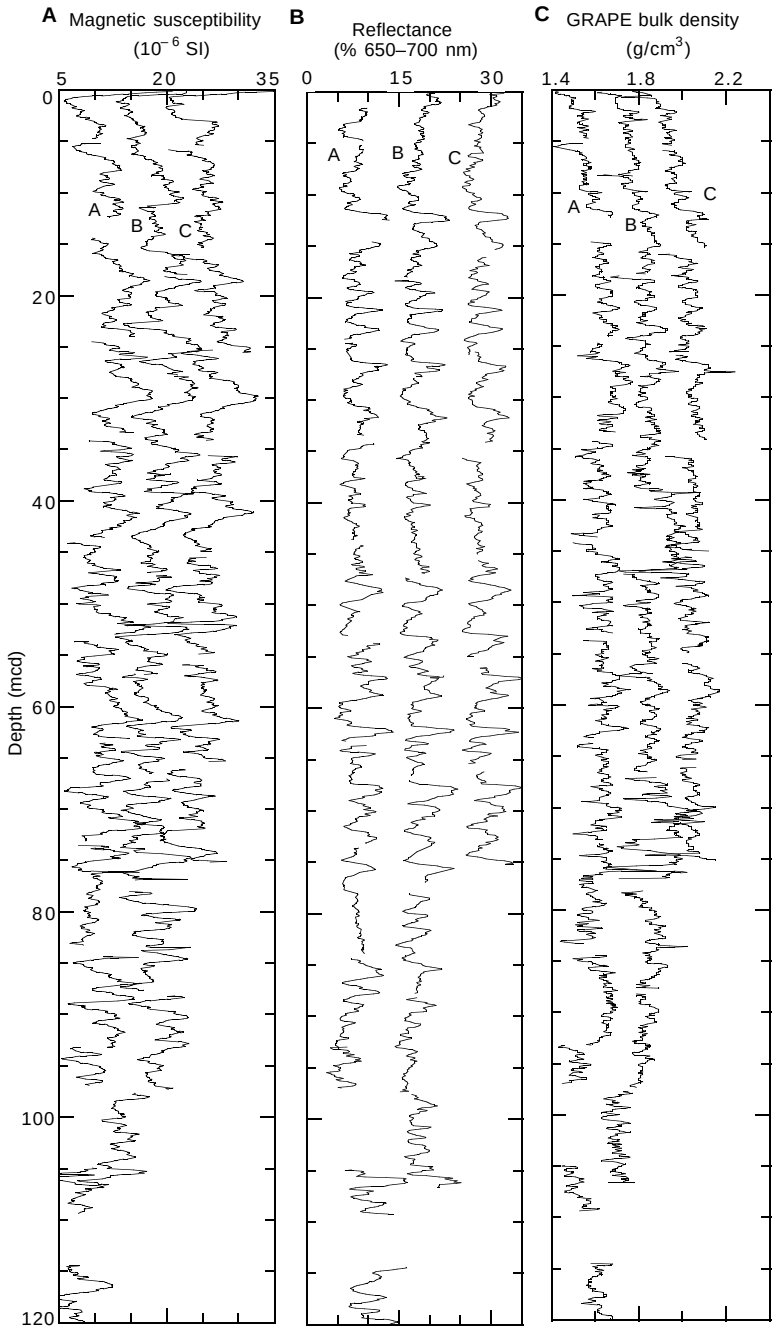

Figure 9. **A.** Smoothed (20-cm Gaussian) magnetic susceptibility data for the upper 120 m from Site 1013 on the mcd scale. Holes 1013A, 1013B, and 1013C are offset from each other by a constant (10×10^{-6} SI). **B.** Smoothed (20-cm Gaussian) color reflectance (% 650–700 nm band) data for the upper 120 m from Site 1013 on the mcd scale. Holes 1013A, 1013B, and 1013C are offset from each other by a constant (10%). **C.** Smoothed (20-cm Gaussian) GRAPE data for the upper 120 m from Site 1013 on the mcd scale. Holes 1013A, 1013B, and 1013C are offset from each other by a constant (0.2 g/cm^3).

from the top to the bottom of the sediment column. TOC varies in a meter to decameter scale, which is also visible in the color of the sediment. Dark greenish intervals display higher organic carbon contents, whereas lighter intervals are carbonate rich and organic-carbon lean. The highest TOC content at 90 mbsf is attributed to both the influx of terrigenous organic matter and less dilution by carbonate, based on its relatively high TOC/TN ratio and low $CaCO_3$ content (Table 12).

Total nitrogen values at Site 1013 vary between 0.16 and 0.69 wt%. Total sulfur content ranges from 0 to ~1.9 wt% (Table 12). Total organic carbon/total nitrogen (TOC/TN) ratios were used to characterize the type of organic matter in the sediments. Most of the TOC/TN are slightly higher than at Sites 1011 and 1012. Values between 10 and 12 suggest a mixture of marine and terrigenous organic matter (Fig. 14; Bordovskiy, 1965; Emerson and Hedges, 1988). A slightly positive correlation between TOC and TOC/TN ratio and a negative

Table 8. Site 1013 splice tie points.

Hole, core, section, interval (cm)	Depth (mbsf)	Depth (mcd)		Hole, core, section, interval (cm)	Depth (mbsf)	Depth (mcd)
				1013B-1H-1, 0	0.00	0.00
1013B-1H-5, 144	7.44	7.44	tie to	1013A-2H-2, 94	7.54	7.44
1013A-2H-4, 29	9.89	9.79	tie to	1013B-2H-2, 9	10.19	9.79
1013B-2H-6, 57	16.67	16.27	tie to	1013A-3H-2, 45	16.55	16.27
1013A-3H-3, 137	18.97	18.69	tie to	1013B-3H-1, 70	18.70	18.69
1013B-3H-6, 65	26.25	26.24	tie to	1013A-4H-2, 40	26.00	26.24
1013A-4H-3, 93	28.03	28.27	tie to	1013B-4H-1, 49	28.09	28.27
1013B-4H-7,59	37.19	37.37	tie to	1013A-5H-3, 35	36.95	37.37
1013A-5H-4, 65	38.78	39.20	tie to	1013B-5H-2, 42	39.02	39.20
1013B-5H-7, 5	46.15	46.33	tie to	1013A-6H-2, 91	45.51	46.33
1013A-6H-4, 23	47.83	48.65	tie to	1013B-6H-1, 149	48.09	48.65
1013B-6H-7, 41	56.01	56.57	tie to	1013C-7H-1, 73	53.93	56.57
1013C-7H-6, 95	61.65	64.29	tie to	1013A-8H-1, 77	62.87	64.29
1013A-8H-3, 95	66.05	67.47	tie to	1013B-8H-1, 46	66.06	67.47
1013B-8H-6, 46	73.56	74.97	tie to	1013A-9H-2, 0	73.10	74.97
1013A-9H-4, 89	76.99	78.86	tie to	1013B-9H-1, 89	75.99	78.86
1013B-9H-5, 133	82.43	85.30	tie to	1013A-10H-1, 101	82.11	85.30
1013A-10H-3, 107	85.17	88.36	tie to	1013B-10H-1, 28	84.88	88.36
1013B-10H-7, 25	93.85	97.33	tie to	1013B-10X-7, 0	93.82	97.33
1013B-11X-6, 61	102.21	105.69	tie to	1013A-12X-1, 89	98.99	105.69
1013A-12X-3, 145	102.55	109.25				

Note: This table is also on CD-ROM, back pocket, this volume.

Table 9. Site 1013 sedimentation rate age control points.

Event	Chron/ subchron	Composite depth (mcd)	Age (Ma)
B Brunhes	C1n	56.64	0.78
T Jaramillo	C1r.1n	65.97	0.99
B Jaramillo	C1r.1n	69.27	1.07
T Olduvai	C2n	92.44	1.77
T *P. lacunosa*		35.66	0.46
T large *Gephyrocapsa* spp.		73.58	1.24
B large *Gephyrocapsa* spp.		85.88	1.44
T *D. tamalis*		148.00	2.76

Note: B = bottom, T = top.

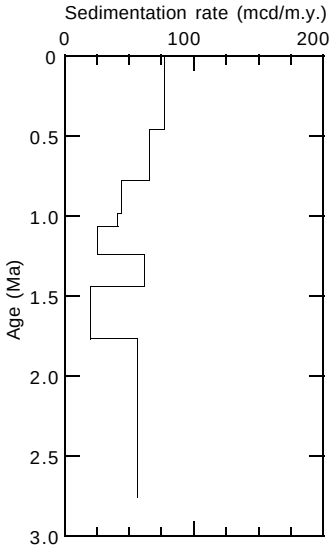

Figure 10. Sedimentation rate vs. age at Site 1013 based on the age control points from Table 9.

correlation between TOC and $CaCO_3$ contents (Fig. 15) indicates that episodic supply of terrigenous organic matter increased the TOC values, and the carbonate dilution decreased their values.

PHYSICAL PROPERTIES

Multisensor Track Measurements

The shipboard physical properties program at Site 1013 included nondestructive measurements of bulk density, magnetic susceptibility, *P*-wave velocity, and natural gamma-ray activity on whole sections of all cores using the MST (Fig. 16). Magnetic susceptibility was measured at 4-cm intervals in all Site 1013 holes at low sensitivity (1-s measuring time). GRAPE bulk density measurements were made at 4-cm intervals in all Site 1013 holes. The PWL velocity measurements were made at 4-cm intervals but gave poor results because of signal attenuation and sediment cracking from high gas content (see "Organic Geochemistry" section, this chapter). PWL measurements were not collected after Sections 167-1013A-5H-7 and 167-1013B-2H-7 and for the entire Hole 1013C. Natural gamma-ray activity was measured with a 15-s count every 12 cm in Holes 1013A and 1013B but was deactivated for Hole 1013C.

Index Properties

Index properties measurements were made at one sample per working section in the first 21 cores and below this at an average of three per core to total depth (TD) in Hole 1013A. Index properties were determined by the gravimetric Method C (see "Physical Properties" section, "Explanatory Notes" chapter, this volume). Values of bulk density and the index properties void ratio, porosity, water content, dry-bulk density, and grain density are presented in Table 13 on CD-ROM in the back pocket of this volume. The properties show little variation downhole, indicating a fairly homogeneous section (Fig. 17), with the few variations most likely corresponding to fluctuating amounts of clay and carbonate (see "Lithostratigraphy" section, this chapter).

Compressional-Wave Velocity

P-wave velocity measurements were made two per core to a depth of 28 mbsf in Hole 1013A. The Hamilton Frame (pair T3) was used exclusively to measure sonic velocity in the x-direction in the first four cores while they were still in the liner (Table 14 on CD-ROM in the back pocket of this volume). Measured velocities range consis-

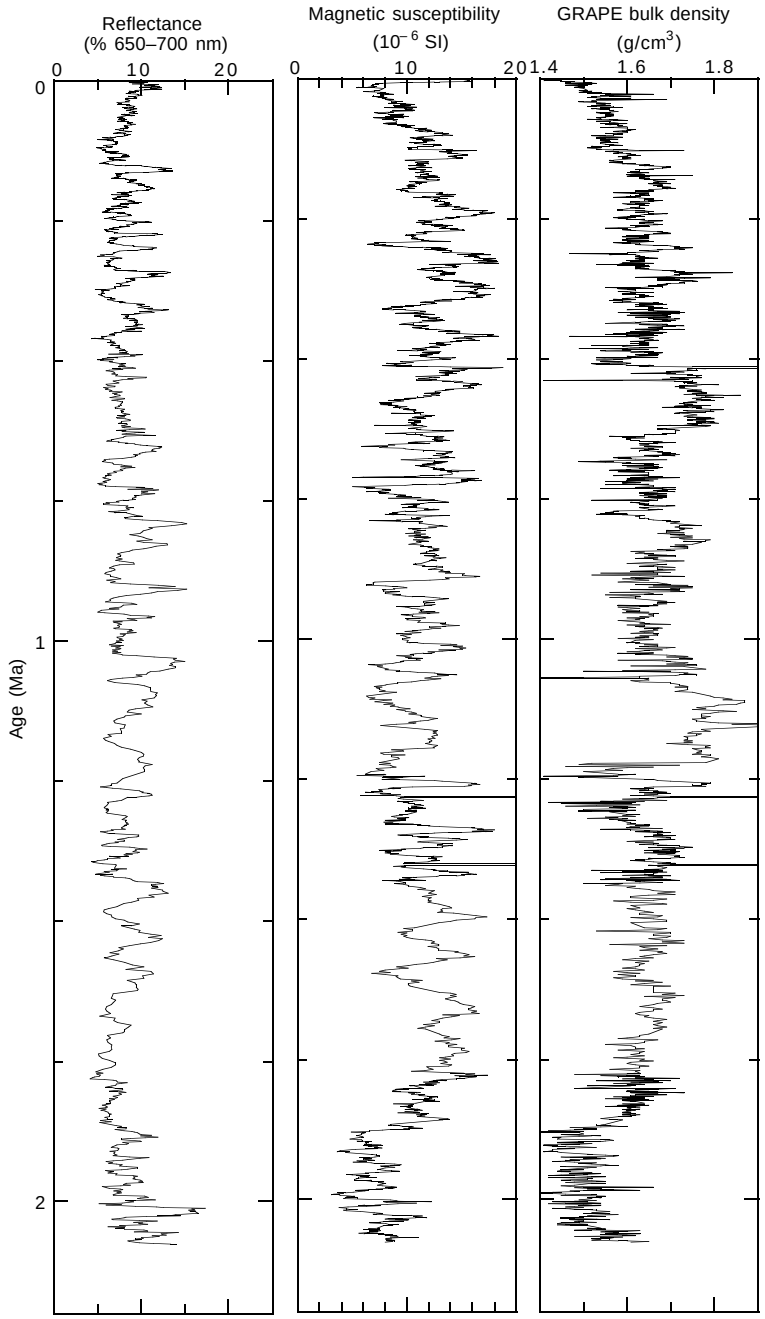

Figure 11. Spliced records of Site 1013 color reflectance, magnetic susceptibility, and GRAPE bulk density vs. age based on age control points from Table 9.

tently between 1563 and 1577 m/s. Unfortunately, below 29 mbsf the sediments became too gassy (see "Organic Geochemistry" section, this chapter), resulting in high signal attenuation that precluded further measurements downhole.

Heat Flow

Thermal conductivity was measured in the sediment cores of Hole 1013C to 70.95 mbsf (Table 15 on CD-ROM in the back pocket of this volume). Three downhole temperature measurements were taken with the APC Adara temperature tool in Hole 1013C: 5.9°C at 34.2 mbsf, 7.8°C at 53.2 mbsf, and 8.6°C at 72.2 mbsf in Cores 167-1013C-4H, 6H, and 8H, respectively (Fig. 18). The bottom-water temperature was measured during the run for Core 167-1013C-4H, leaving the tool at the mudline for approximately 6.5 min before piston coring. The data indicate a bottom-water temperature of 3.6°C ± 0.1°C. The four data points yield a thermal gradient of 72°C/km (Fig. 19). Using an average measured thermal conductivity of 0.897 W/(m·K) provides a heat-flow estimate of 65 mW/m^2 at Site 1013.

Color Reflectance

Reflectance measurements were taken at 4-cm intervals to 33 mbsf in Hole 1013A and at 6-cm intervals for the remainder of Hole 1013A and all of Holes 1013B and 1013C. Color reflectance values are generally lower at Site 1013 than at Site 1012, most likely because of the higher organic carbon content at Site 1013 (see "Organic Geochemistry" section, this chapter). A composite color reflectance

Table 10. Interstitial water geochemical data, Hole 1013A.

Core, section, interval (cm)	Depth	pH	Alkalinity (mM)	Salinity	Cl^- (mM)	Na^+ (mM)	SO_4^{2-} (mM)	HPO_4^{2-} (μM)	NH_4^+ (mM)	H_4SiO_4 (μM)	Ca^{2+} (mM)	Mg^{2+} (mM)	Sr^{2+} (μM)	Li^+ (μM)	K^+ (mM)
167-1013A-															
1H-2, 145–150	2.95	7.51	3.41	35.0	548	471	26.8	7	0.3	304	10.2	51.7	86	28	9.9
2H-3, 145–150	9.55	7.48	26.4	34.0	571	493	12.4	106	2.7	567	6.97	52.8	93	30	10.1
3H-3, 145–150	19.05	7.83	46.1	34.0	559	489	1.5	173	4.7	744	4.01	50.3	118	31	10.6
4H-2, 145–150	27.05	7.65	48.6	34.0	554	484	<1	161	5.9	748	3.79	50.1	123	38	10.6
5H-3, 145–150	38.05	7.70	48.6	34.0	564	496	<1	141	10.1	767	3.45	49.5	127	48	10.6
6H-2, 145–150	46.05	7.60	51.0	34.0	563	497	<1	103	10.1	865	3.61	49.3	134	60	10.7
9H-3, 145–150	76.05	7.00	49.3	34.5	555	491	<1	96	10.6	1068	5.24	44.8	170	102	12.8
12X-2, 145–150	101.05	7.01	60.7	36.0	567	506	<1	87	12.3	1063	5.11	50.2	198	136	10.8
15X-3, 145–150	131.35	6.84	56.3	36.0	572	508	<1	59	13.3	1059	6.41	48.4	211	150	11.1

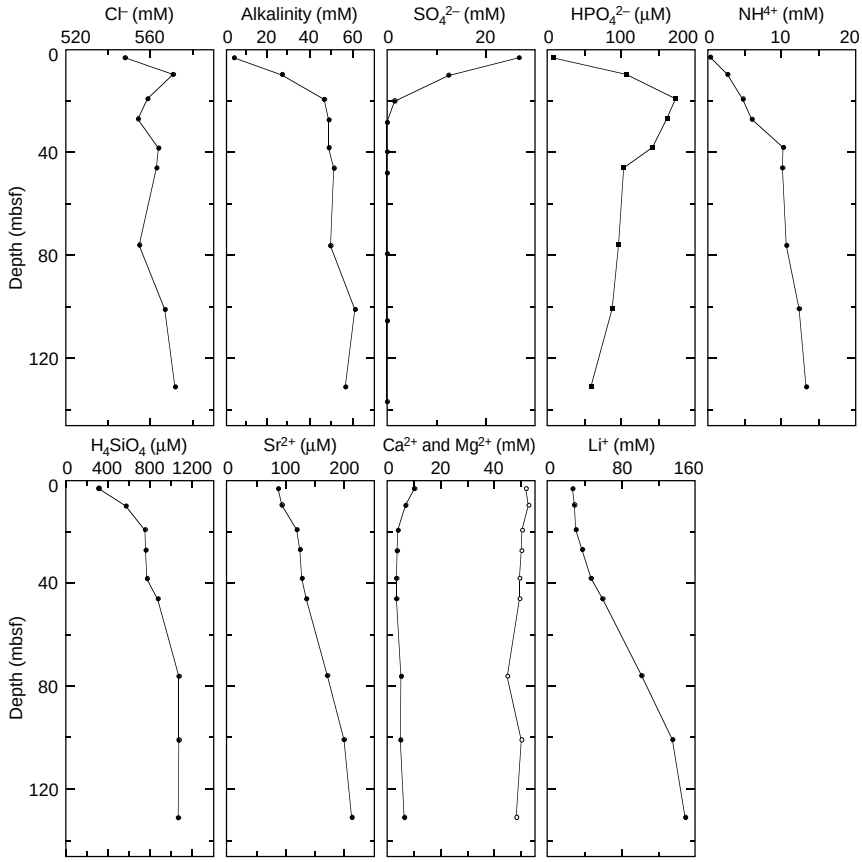

Figure 12. Interstitial water geochemical data, Site 1013. Solid circles = Ca, open circles = Mg.

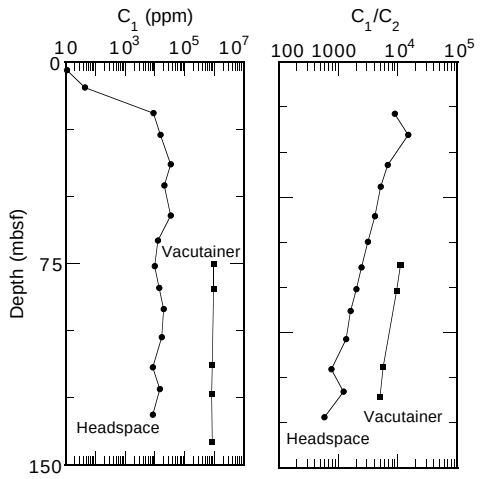

Figure 13. Concentrations of methane (C_1) and methane/ethane (C_1/C_2) ratios obtained by the headspace and vacutainer techniques from Hole 1013A.

record for the 650- to 700-nm band average is included in the "Composite Depths and Sedimentation Rates" section (this chapter). Reflectance data from Hole 1013A were used to predict calcium carbonate content. Two separate regression equations were used, one based on Site 1011 color reflectance and calcium carbonate data and the other from Site 1012. A comparison of the downhole predictions and measured calcium carbonate data is presented in Figure 20.

The two different regressions were used to compare the relative effects of organic carbon on calcium carbonate predictions. Organic carbon values are generally higher at Site 1013 (average ~3.9%) than at Site 1012 (average ~2.6%), both of which are higher than at Site 1011 (average ~1.5%). The Site 1012 equation predicts Site 1013 carbonate relative to the measured values ($r^2 = 0.80$) better than the Site 1011 equation ($r^2 = 0.69$). Calcium carbonate content is generally underestimated using the Site 1011 equation, which most likely results from the lower organic carbon values of this calibration data set. In the future, using equations that take into account the effect of both calcium carbonate and organic carbon content should improve the accuracy of color reflectance-based regressions.

Table 11. Concentrations of methane (C_1), ethene ($C_{2=}$), ethane/ethylene (C_2), propane/propylene (C_3), and n-pentane (n-C_5) obtained by the headspace and vacutainer techniques from Hole 1013A.

Core, section, interval (cm)	Depth (mbsf)	C_1 (ppm)	$C_{2=}$ (ppm)	C_2 (ppm)	C_3 (ppm)	n-C_5 (ppm)	C_1/C_2
Headspace							
167-1013A-							
1H-3, 0–5	3.03	11					
2H-4, 0–5	9.63	44					
3H-4, 0–5	19.13	8,995		1			8,995.00
4H-3, 0–5	27.13	14,966		1			14,966.00
5H-4, 0–5	38.13	33,759	1	5	1		6,751.80
6H-3, 0–5	46.13	20,729		4			5,182.25
7H-4, 0–5	57.13	33,481	1	8	3		4,185.13
8H-4, 0–5	66.63	12,706		4			3,176.50
9H-4, 0–5	76.13	9,894		4			2,473.50
10H-3, 0–5	84.13	14,044		7	2		2,006.29
11X-2, 0–5	92.13	19,239	1	12	5		1,603.25
12X-3, 0–5	101.13	17,432	1	13	5		1,340.92
13X-5, 0–5	113.73	8,508	1	11	5		773.45
14X-4, 0–5	121.83	14,910	1	12	5		1,242.50
15X-4, 0–5	131.43	8,689	3	15	10		579.27
Vacutainer							
167-1013A-							
9H-3, 50–51	75.11	938,365	1	84	8	4	11,171
10H-3, 50–51	84.61	993,837		99	10		9,479
13X-4, 50–51	112.71	845,658		149	17	3	5,676
14X-5, 50–51	123.81	804,011		160	20	3	5,025
16X-4, 50–51	141.51	855,262		190	23		

Table 12. Depth variations in concentrations of total carbon, inorganic carbon, total organic carbon, calcium carbonate, total nitrogen, and total sulfur in weight percent (wt%) in Hole 1013A.

Core, section, interval (cm)	Depth (mbsf)	Inorganic carbon (wt%)	$CaCO_3$ (wt%)	Total carbon (wt%)	Total organic carbon (wt%)	Total nitrogen (wt%)	Total sulfur (wt%)	Total organic carbon/total nitrogen	Total organic carbon/total sulfur
167-1013A-									
1H-1, 36–37	0.36	2.52	20.99	6.96	4.44	0.50	0.00	8.88	
1H-2, 29–30	1.79	2.49	20.74	7.01	4.52	0.45	1.63	10.04	2.77
1H-3, 29–30	3.29	2.02	16.83	5.97	3.95	0.38	1.68	10.39	2.35
2H-1, 31–32	5.41	2.42	20.16	7.30	4.88	0.46	1.81	10.61	2.70
2H-2, 30–31	6.90	1.82	15.16	6.33	4.51	0.43	1.21	10.49	3.73
2H-3, 30–31	8.40	0.91	7.58	5.76	4.85	0.48	1.38	10.10	3.51
2H-4, 30–31	9.90	1.78	14.83	8.44	6.66	0.62	1.61	10.74	4.14
2H-5, 30–31	11.40	0.73	6.08	7.04	6.31	0.58	1.82	10.88	3.47
3H-1, 109–110	15.69	2.81	23.41	6.65	3.84	0.36	1.09	10.67	3.52
3H-2, 29–30	16.39	2.38	19.83	7.13	4.75	0.55	1.36	8.64	3.49

Only part of this table is produced here. The entire table appears on the CD-ROM.

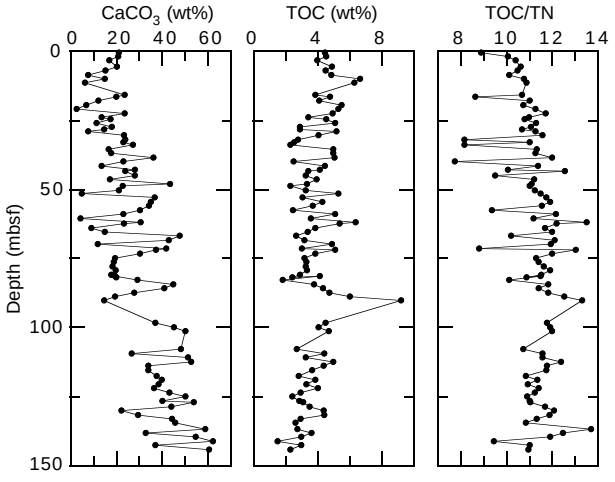

Figure 14. Depth variations of calcium carbonate ($CaCO_3$), total organic carbon (TOC) content, and total organic carbon/total nitrogen (TOC/TN) in sediments of Hole 1013A.

Digital Color Video

Cores from Hole 1013A were imaged with the ODP digital color imaging system over 20-cm intervals to provide a 0.25-mm pixel.

SUMMARY

At Site 1013, in the San Nicolas Basin of the California Borderland, we drilled a high-resolution, upper Neogene sedimentary section designed to sample upper intermediate waters at the basin sill depth of 1100 mbsl, although the actual depth of the drill site is 1564 mbsl (Fig. 21). Based on their sill depths, Sites 1011, 1012, and 1013 form a transect for intermediate water study from ~1600 mbsl to 1100 mbsl. At Site 1013, the interval 0–74 mbsf (~0–1.3 Ma) was triple cored, 74-104 mbsf (~1.3–1.9 Ma) was double cored, and 104–146 mbsf (~1.9–2.7 Ma) was single cored, with a continuous sedimentary sequence documented to 94 mbsf (~1.7 Ma). A good paleomagnetic reversal sequence and calcareous biostratigraphy form the primary stratigraphy at Site 1013. The only siliceous fossils present were reworked and of middle Miocene age. The high quality of the paleomagnetic record was surprising, as it was at Site 1012, because of the high sedimentary organic carbon content (averaging ~4%) and the significant organic matter diagenesis within the sediment column, as

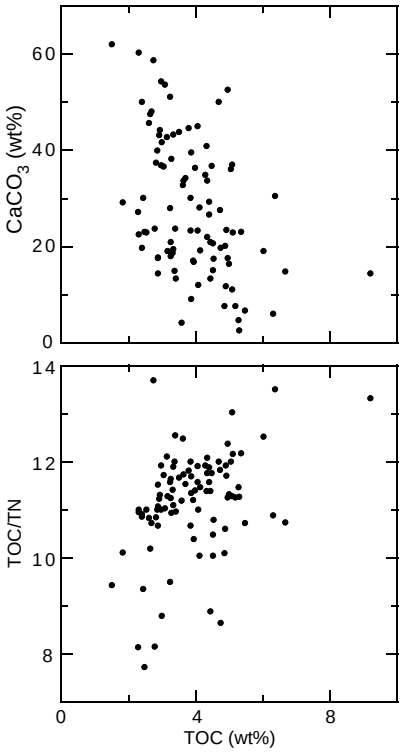

Figure 15. Plots of TOC/TN ratio and $CaCO_3$ content vs. total organic carbon content (TOC) in sediments of Hole 1013A.

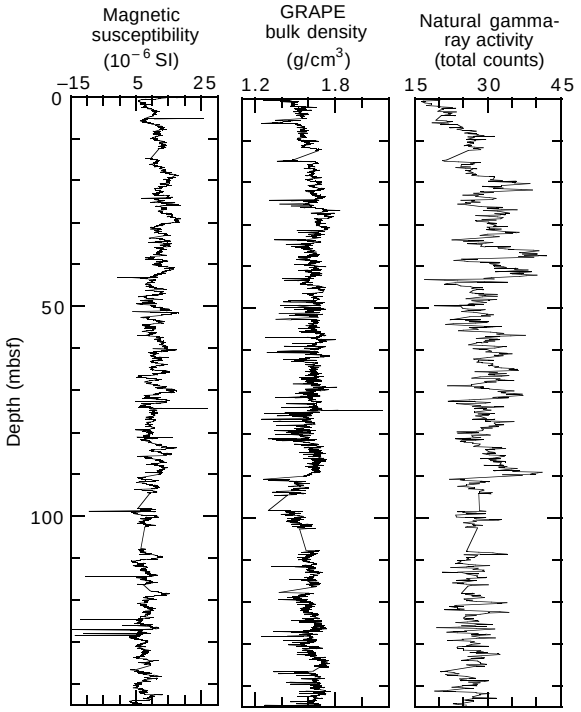

Figure 16. MST data from Hole 1013A.

indicated by the interstitial water analyses. Typical magnetic minerals should have been reduced by diagenetic reactions in the upper sediment column.

Site 1013 has a very similar sedimentary column to Site 1012, which is to be expected because of the proximity of the two sites (68 km) and their similar sedimentary environments. Distinctive features to note within the lithostratigraphic column at Site 1013 are the lack of siliceous microfossils and the high calcium carbonate contents in the Pliocene section, which decrease by over half by the upper Pleistocene sediments. The drilled section did not reach the acoustically reflective units (Fig. 21), which presumably are diagenetic dolomites.

REFERENCES

Bordovskiy, O.K., 1965. Accumulation and transformation of organic substances in marine sediment, 2. Sources of organic matter in marine basins. *Mar. Geol.*, 3:5–31.

Cande, S.C., and Kent, D.V., 1995. Revised calibration of the geomagnetic polarity timescale for the Late Cretaceous and Cenozoic. *J. Geophys. Res.*, 100:6093–6095.

Emerson, S., and Hedges, J.I., 1988. Processes controlling the organic carbon content of open ocean sediments. *Paleoceanography*, 3:621–634.

Emery, K.O., 1960. *The Sea Off Southern California: A Modern Habitat of Petroleum:* New York (Wiley).

Lyle, M., Gallaway, P.J., Liberty, L.M., Mix, A., Stott, L., Hammond, D., Gardner, J., Dean, W., and the EW9504 Scientific Party, 1995a. Data submission. W9406 and EW9504 site surveys of the California margin proposed drillsites, Leg 167 (Vol. 1): Site maps and descriptions. Boise State Univ., *CGISS Tech. Rep.*, 95–11.

Lyle, M., Gallaway, P.J., Liberty, L.M., Mix, A., Stott, L., Hammond, D., Gardner, J., Dean, W., and the EW9504 Scientific Party, 1995b. Data submission. W9406 and EW9504 site surveys of the California margin proposed drillsites, Leg 167 (Vol. 2): Seismic profiles. Boise State Univ., *CGISS Tech. Rep.*, 95–12.

Ms 167IR-107

NOTE: For all sites drilled, core-description forms ("barrel sheets") and core photographs can be found in Section 3, beginning on page 499. Smear-slide data can be found in Section 4, beginning on page 1327. See Table of Contents for material contained on CD-ROM.

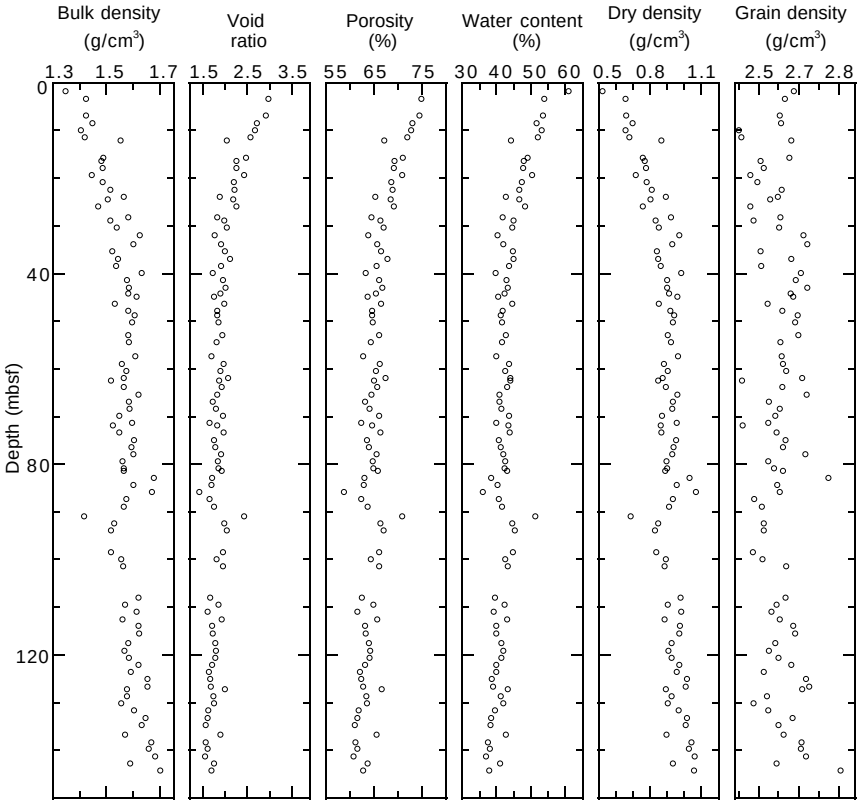

Figure 17. Index properties data from Hole 1013A.

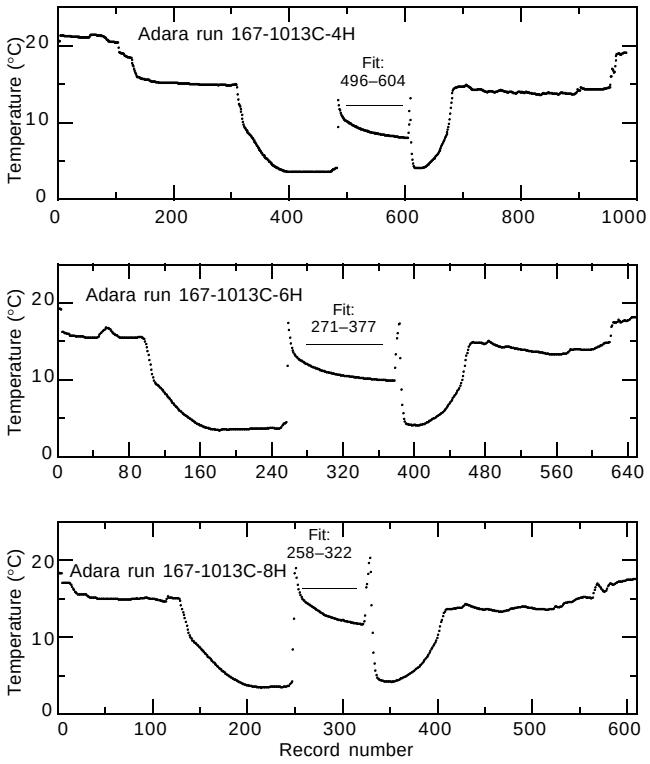

Figure 18. Hole 1013C downhole temperature vs. record number (5-s recording frequency) for each measurement run, showing the interval fitted to determine the downhole temperature.

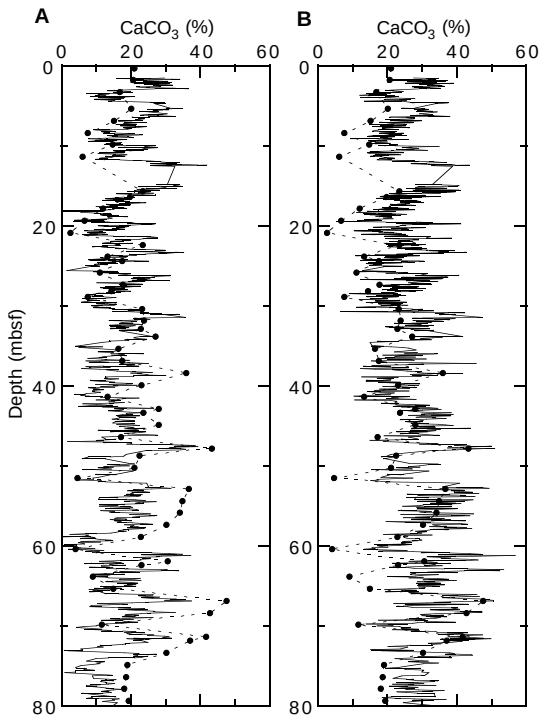

Figure 20. Summary of measured and estimated calcium carbonate values from Hole 1013A. **A.** Based on Site 1011 regression (solid line = estimated values, dashed line connects measured values). **B.** Based on Site 1012 regression (symbols as in part A).

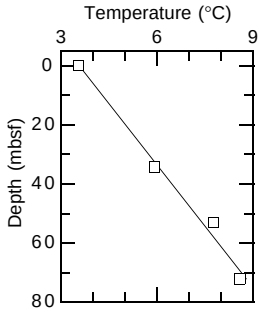

Figure 19. Downhole temperature gradient for Hole 1013C.

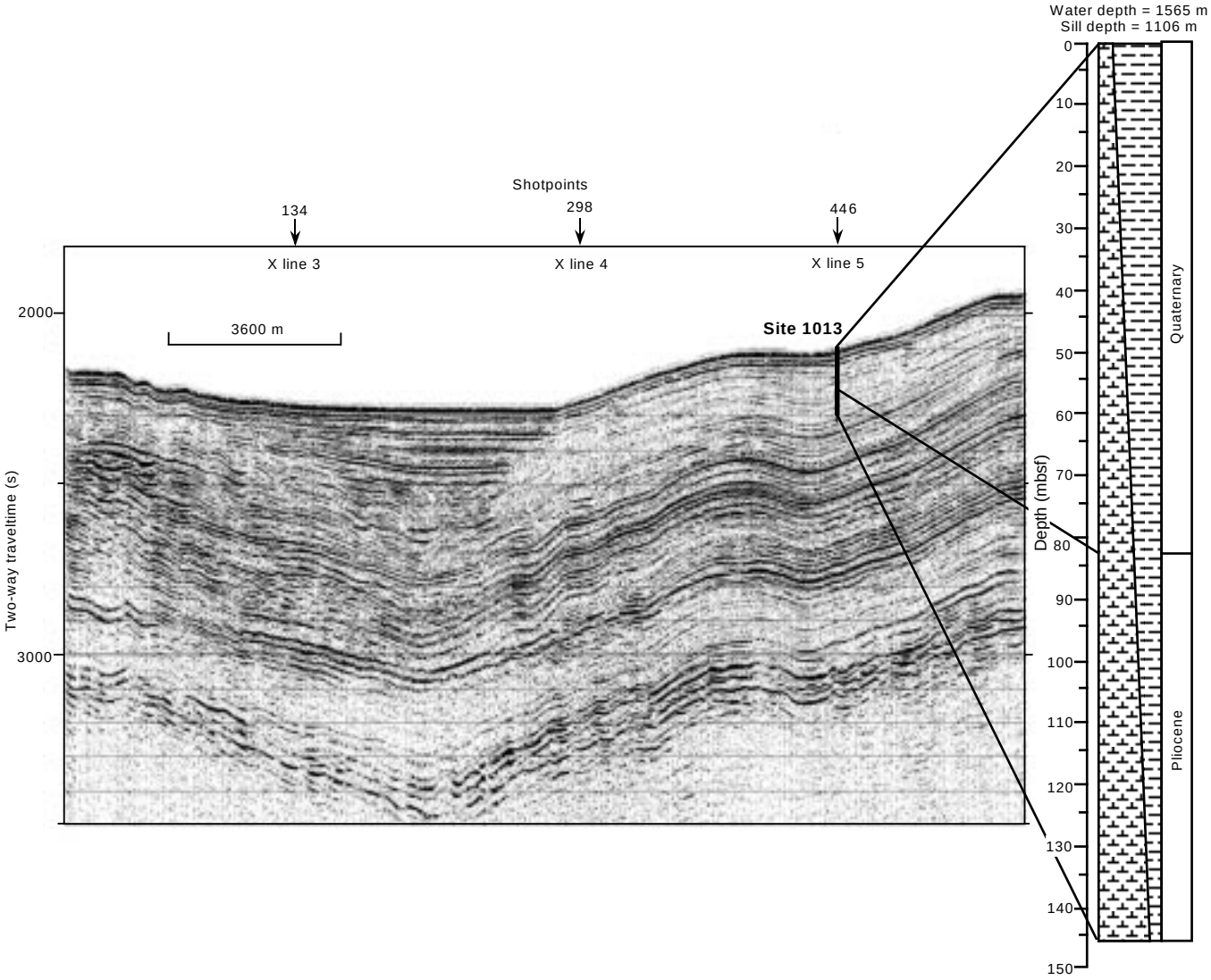

Figure 21. Comparison of the lithostratigraphic column at Site 1013 and a seismic profile through the site (Line EW9504 BA2-1; Lyle et al., 1995a, 1995b). Ties are calculated from measured seismic velocities (see “Physical Properties” section, this chapter). On y-axis, (s) = milliseconds.

Previous Chapter Table of Contents Next Chapter